Low divergence proton beams from a laser-plasma accelerator at kHz repetition rate

Dan Levy, Igor Andriyash, Stefan Haessler, Jaismeen Kaur, Marie Ouillé, Alessandro Flacco, Eyal Kroupp, Victor Malka, Rodrigo B. Lopez-Martens

Low divergence proton beams from a laser-plasma accelerator at kHz repetition rate

Dan Levy,[1,*] Igor A. Andriyash,[2,†] Stefan Haessler,[2,‡] Jaismeen Kaur,[2] Marie Ouillé,[2,3] Alessandro Flacco,[2] Eyal Kroupp,[1] Victor Malka,[1] and Rodrigo Lopez-Martens[2]

[1]*Department of Physics of Complex Systems, Weizmann Institute of Science, Rehovot 76100, Israel*
[2]*Laboratoire d'Optique Appliquée, ENSTA Paris, CNRS, Ecole Polytechnique, Institut Polytechnique de Paris, 828 Bd des Maréchaux, 91762 Palaiseau, France*
[3]*Ardop Engineering, Cité de la Photonique, 11 Avenue de la Canteranne, Bât. Pléione, 33600 Pessac, France*

(Received 13 December 2021; revised 6 July 2022; accepted 1 September 2022; published 26 September 2022)

Proton beams with up to 100 pC bunch charge, 0.48 MeV cutoff energy, and divergence as low as 3° were generated from solid targets at kHz repetition rate by a few-mJ femtosecond laser under controlled plasma conditions. The beam spatial profile was measured using a small aperture scanning time-of-flight detector. Detailed parametric studies were performed by varying the surface plasma scale length from 8 to 80 nm and the laser pulse duration from 4 fs to 1.5 ps. Numerical simulations are in good agreement with observations and, together with an in-depth theoretical analysis of the acceleration mechanism, indicate that high repetition rate femtosecond laser technology could be used to produce few-MeV proton beams for applications.

DOI: 10.1103/PhysRevAccelBeams.25.093402

Over the past two decades, ion acceleration with intense femtosecond laser pulses has emerged as a promising alternative to conventional accelerators due to its much higher instantaneous flux, potentially lower costs, and smaller facility size. Laser-accelerated protons are already used for target studies for fast ignition [1], studies of warm dense matter [2], and probing fast phenomena in laser-matter interaction [3]. However, societal applications of laser-accelerated protons such as proton therapy [4] and nuclear physics research [5] require source parameters that are still out of reach for existing laser-based accelerators [6,7]. Intense research efforts are dedicated to improving the source performance in terms of particle energy, average flux, beam brightness, and overall source efficiency.

Ion acceleration with ultraintense lasers ($I_{las} \gtrsim 10^{18}$ W/cm^2) is currently mostly realized by irradiating thin (~0.1–10 μm) foils, utilizing the well-known target normal sheath acceleration (TNSA) mechanism [8,9] which is driven by the thermal pressure of hot electrons generated by the laser. Commercially available 100-TW-class lasers deliver TNSA proton beams with energies reaching up to a few tens of MeV and 10^{11}–10^{13} protons per shot above 1 MeV, depending on target and laser parameters [10]. These lasers typically operate at 1–10 Hz, yet a continuous operation with thin foils at this rate is very challenging due to target replenishing needs and debris contamination in the vacuum chamber.

Another major shortcoming of TNSA proton beams compared to the ones from conventional accelerators is their much larger divergence, which ranges from 10° to 30° FWHM [11–13]. The demand for high brightness has driven considerable research efforts aiming at reducing the angular spread of laser-generated beams. Such efforts include additional collimation devices [14–16], special target geometries [8,17–30], and targets that enable other acceleration mechanisms [31–35]. In many cases, target fabrication and handling, together with stringent laser contrast requirements for laser-solid acceleration, hinder the use of these targets in applications where a stable operation at a high repetition rate is necessary.

With the latest advancements in laser technology, ion acceleration using kHz lasers is emerging as a promising path for generating proton beams of sufficient flux and energy. Studies include both solid targets [36,37] as well as other types. Recently, Morrison *et al.* demonstrated kHz proton beams of up to 2 MeV using a mJ-class laser and a thin liquid sheet target [38]. Beam divergence with this target remains however similar to typical TNSA beams and thus remains a serious limitation for practical use.

In this paper, we demonstrate and analyze a robust, efficient, and easy-to-implement method for delivering

*dan.levy@weizmann.ac.il
†igor.andriyash@ensta-paris.fr
‡stefan.haessler@cnrs.fr

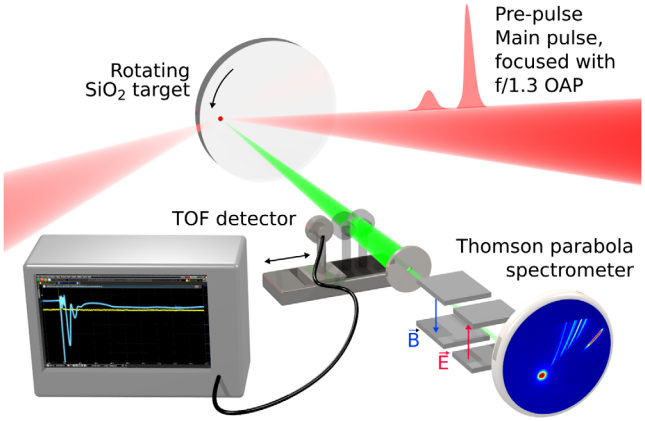

FIG. 1. Experimental setup.

highly collimated proton beams at kHz repetition rate using few-mJ femtosecond pulses. The underlying mechanism is essentially different from TNSA, and its previous studies suggested that it is associated with electron motion in the Brunel heating process [37]. We revisit this process experimentally with vastly improved laser performance in terms of intensity and temporal contrast. In addition, we measure for the first time the angular and energy distributions of the accelerated protons over a wide range of interaction conditions by varying both pulse duration and plasma gradient length. The obtained data were used to construct a comprehensive theoretical description supported by detailed numerical modeling. Our findings give a clear physical picture of the acceleration and its scalability for applications.

The experiment was carried out at the Salle Noire facility of Laboratoire d'Optique Appliquée (LOA). The laser delivers 27 fs pulses at a 1-kHz repetition rate with high temporal contrast ($> 10^{10}$ at 10 ps). The pulse duration can be reduced to 4 fs in a hollow-fiber compressor [39] and increased up to 1500 fs by adding intrachain group delay dispersion (GDD), while keeping the same energy and spatial intensity distribution on target. The peak intensity on target can thus be tuned from 10^{16} to 10^{19} W/cm^2. A schematic layout of the experiment is shown in Fig. 1, where the 2.5 mJ, p-polarized pulses are focused by an $f/1.3$, 30° off-axis parabolic mirror (OAP) down to a $R_{\mathrm{las}} \approx 1.8$ μm FWHM focal spot at 55° incidence angle at the surface of a rotating fused silica optical substrate. A time-delayed prepulse is added by picking off ≈4% of the main pulse through a holey mirror and focusing it with the same OAP to a larger 13 μm FWHM spot. The preplasma gradient scale length $L_g \approx L_0 + c_s t_d$ can be controlled by changing the relative delay t_d between the prepulse and the main pulse, where L_0 corresponds to an additional expansion induced by the main pulse pedestal due to its finite temporal contrast. The plasma expansion velocity c_s is measured using spatial domain interferometry (SDI) [40]. The high-stability rotating target holder [41] keeps the target surface position stable within the few-micron Rayleigh length of the tightly focused main pulse while refreshing the target surface for shots at 1 kHz.

The proton energy and angular distributions were measured with a Thomson parabola spectrometer (TPS) and a charge-calibrated scanning time-of-flight (TOF) detector. The TPS accepts ions in the normal direction through a 300-μm pinhole placed at about 0.6 m from the target. The TOF detector consists of a 6-mm diameter microchannel plate (MCP) placed 375 mm away from the irradiated point and connected to an 8-GHz oscilloscope. This setup provides an acceptance angle of 0.9°, such that the broadening of the measured angular profile due to convolution with the detector size is negligible. To the best of our knowledge, this is the first time a TOF detector was used to measure the angular distribution of the beam. Further details regarding both detectors are available in the Supplemental Material [42].

Figures 2(a) and 2(b) show proton energy spectra acquired with the TPS, where each spectrum is an average of 100 consecutive shots. In Fig. 2(a), the pulse duration is fixed at $\tau_{\mathrm{las}} = 27$ fs and the prepulse delay is varied. The highest proton energies around 0.25 MeV are achieved for the steepest gradient and drop below the detection threshold of 0.1 MeV for the gradients $L_g \gtrsim \lambda/6$. In Fig. 2(b), the gradient is kept the steepest (0 ps delay) and the pulse duration is varied. We observe an optimum around 100–300 fs, where the maximum proton energy W_{max} reaches 0.48 ± 0.02 MeV. For the longer pulses, the maximum proton energy slowly decreases.

Figures 2(c)–2(e) show the angle-resolved TOF spectra measured for the sharpest plasma gradient and for driving pulse durations of 4, 27, and 200 fs. For each angle, each spectrum shown is an average of 100 consecutive shots. All three measurements in Figs. 2(c)–2(e) show similar angular profiles and in all cases, the energy-integrated divergence is ≈3° (FWHM). Assuming a two-dimensional Gaussian angular profile, we calculate the total charge (above 0.1 MeV) to be 12 ± 2.4, 50 ± 10, and 98 ± 20 pC, respectively. The single-axis measurement is indeed fitted very well by a Gaussian and we expect the beam asymmetry to be small due to the symmetry of the system, as was observed in [36] (albeit with much larger beam divergence). Our estimation of a 20% error originates from uncertainties in the angular distribution and the TOF calibration, as described in the Supplemental Material [42].

Figure 2 points out that the acceleration benefits from the shortest, laser-contrast-limited plasma gradient, and that the highest cut-off energies are reached for $\tau_{\mathrm{las}} \sim$ 100–200 fs, at the point when the growth $W_{\mathrm{max}} \propto \tau_{\mathrm{las}}$ switches to a slow decrease $W_{\mathrm{max}} \propto I_{\mathrm{las}} \propto 1/\tau_{\mathrm{las}}$. This first regime suggests that for the short pulses, the acceleration is directly driven by the laser-plasma interaction, while not strongly depending on the laser intensity. Let us consider a physical picture of a solid plasma slab irradiated obliquely by a short subrelativistic

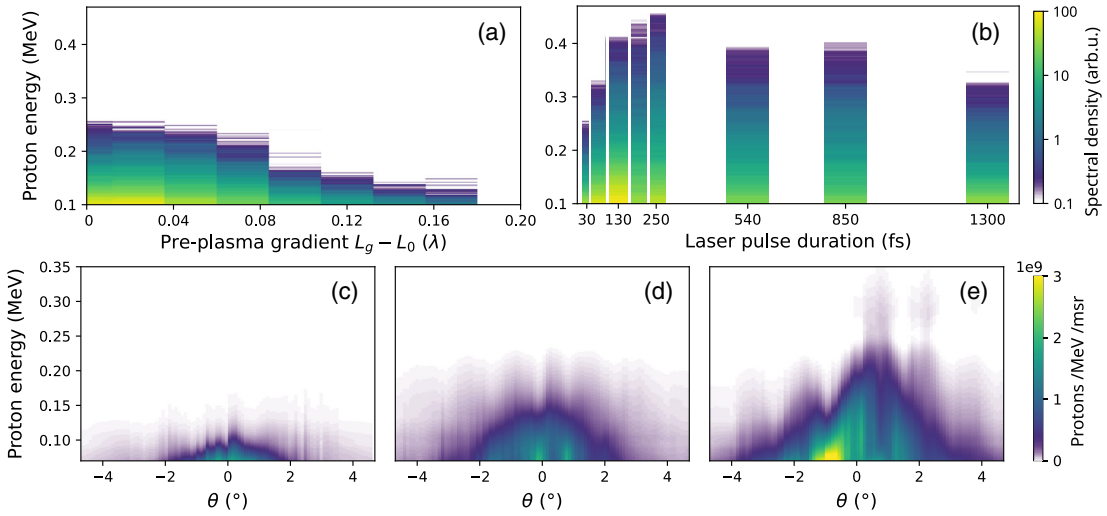

FIG. 2. TPS proton spectra in arbitrary units and logarithmic scale, for $\tau_{las} = 27$ fs and varying plasma scale length (a), and for 0 prepulse delay and varying pulse duration (b). Angular-spectral proton number distributions measured with the calibrated TOF detector for 4 fs (c), 27 fs (d), and 200 fs (e).

laser pulse, with field strength $a_0 = eE_{las}\lambda/2\pi m_e c^2 < 1$, where $E_{las} = \sqrt{2I_{las}/\epsilon_0 c}$ is the peak electric field, λ is its wavelength, e and m_e are the electron charge and mass, respectively, and c is the speed of light in vacuum. The laser field penetrates the preplasma until it reaches the reflective layer with electron density $n_{pe} \gtrsim n_c$, where $n_c = \pi/r_e\lambda^2$ is the critical plasma density and r_e is the classical electron radius. Within this layer, the laser introduces the radiation pressure $P_{rad} = 2\cos^2\theta\, I_{las}/c$, which expels plasma electrons until it becomes balanced by the electrostatic pressure P_{es}. For a short preplasma gradient, $L_g \ll \lambda$, the laser and electrostatic fields beyond the penetrated layer are instantly screened by the dense plasma, enabling the well-known Brunel absorption [43]. Owing to this screening, electrons escape deep into the plasma without building up a dense negative layer, thus allowing ions to generate a long-range accelerating field. For the considered laser intensities, the preplasma consists of only partially ionized Si, O, and C ions, and a small fraction of protons (see Sec. IC and S-Fig. 3 in the Supplemental Material [42]). The latter has a much higher charge-to-mass ratio than heavier ions, $1/m_p \gg Z_i/M_i$ and can thus be quickly accelerated in the electrostatic field of this positively charged preplasma before its own Coulomb explosion.

Let us now consider a simple quantitative description of the physical process described above. We assume a plasma with initial density, $n_{p0} \gg n_c$, that is uniform for $z < 0$, and falls as $n_p = n_{p0}\exp(-z/L_g)$ for $z > 0$. The thickness of the un-neutralized ion layer created by the laser pressure can be estimated from the balance condition, $P_{es} \simeq P_{rad}$, as:

$$z_0 \simeq L_g \ln\left(\frac{en_{p0}L_g}{2\cos\theta}\sqrt{\frac{c}{\epsilon_0 I_{las}}}\right), \tag{1}$$

where ϵ_0 is the vacuum permittivity (for details see [42]). For $z > z_0$, the field profile can be estimated theoretically by considering the model of a thin charged disk:

$$E_z(t,z) = \frac{\hat{E}_{las}(t)\cos\theta}{2}\left[1 - \exp\left(-\frac{z-z_0}{L_g}\right)\right] \times \left(1 - \frac{z}{\sqrt{z^2 + R_i^2}}\right), \tag{2}$$

where $\hat{E}_{las}$ is the amplitude of the laser electric field, and the size of the charged ion disk is determined by the projected laser spot size as $R_i = R_{las}/\cos\theta$. In the particular limit when the acceleration length is short compared to the field's scale R_i and long compared to the preplasma scale L_g, one may discard the geometric factors in Eq. (2) and calculate the proton energy obtained in the field $E_z = \hat{E}_{las}(t)\cos\theta/2$ over the laser duration as

$$W_{max} = \sqrt{\frac{\ln 2}{\pi}}\frac{e^2}{m_p c\,\epsilon_0}\frac{W_{las}\,\tau_{las}}{R_i^2}, \tag{3}$$

where W_{las} is the laser energy. Noting that the field in Eq. (2) vanishes for $z \gtrsim R_i/2$, and limiting the full interaction time by $2\tau_{las}$, we can define the validity condition for Eq. (3) as $\langle v_p\rangle\tau_{las} \lesssim R_i/4$, where $\langle v_p\rangle = \sqrt{W_{max}/2m_p}$ is the proton velocity averaged over the acceleration duration. At its limit, this condition defines a case when protons reach the vanishing field by the end of the interaction, and it thus defines the optimal acceleration regime. Applying this condition to Eq. (3), we obtain the scaling

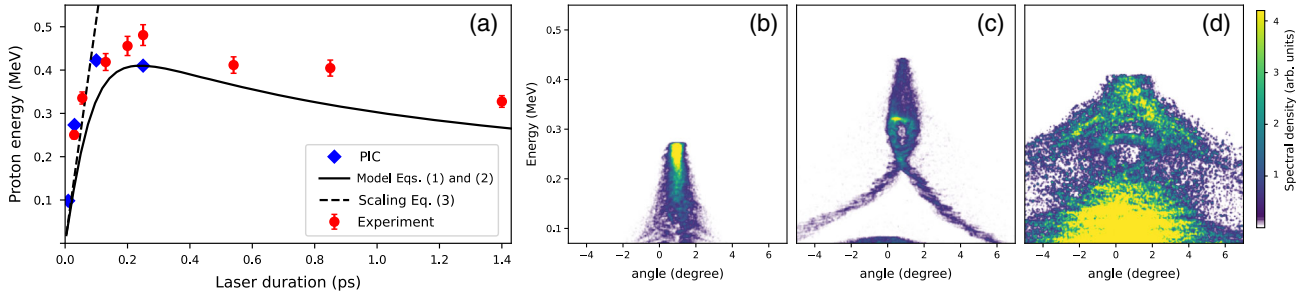

FIG. 3. (a) Maximum proton energy as a function of laser pulse duration obtained experimentally (red dots), in PIC simulations (blue diamonds), from numerical integration of proton motion with Eq. (1) and (2) (black solid line), and the scaling Eq. (3) (dashed line). (b–d) Final angular spectral distributions of protons for 30 fs (b), 100 fs (c) and 250 fs (d) laser pulse durations.

$$W_{\mathrm{opt}} = \left(\sqrt{\frac{2\ln 2}{\pi m_p}}\,\frac{e^2}{4c\,\epsilon_0}\,\frac{W_{\mathrm{las}}}{R_{\mathrm{i}}}\right)^{2/3}, \tag{4}$$

which suggests that the maximum cutoff energy depends neither on the plasma nor on the preplasma features (as long as $L_{\mathrm{g}} \ll \lambda$) but is determined solely by the laser energy and its projected spot size. More details on the theoretical analysis can be found in [42].

The described mechanism relies on the persisting I_{las}, and as soon as the laser pressure is gone, electrons flow back into the charge separation region and can drive a consequent TNSA process. For a short preplasma and a short laser, the electrons that refill that region are cold, and this remnant acceleration turns out to be insignificant. For the longer laser pulses, the expansion of the heavier ions breaks the sharp plasma interface, and TNSA occurs during the laser action. This can also be observed in Figs. 2(c)–2(e), where the short-pulse cases (c,d) show all energies being contained within 2° half-angle, while in the 200-fs laser case Fig. 2(e), the angular divergence of protons with $W_p < 0.15$ MeV increases. We note that the TOF measurements in the latter case also indicate that low energy protons (below 0.07 MeV) get intermixed with heavier ions, resulting in an increased divergence of the aggregate signal (up to 5° FWHM). This divergence degradation at longer interaction times cannot be easily avoided, and it restricts the optimal laser durations to not exceed 100–200 fs (weakly depending on the ion composition).

For more details and to verify this interpretation, we consider 2D particle-in-cell (PIC) simulations using the code WarpX [44]. In the simulations, the preplasma has an exponential profile with $L_{\mathrm{g}} = 8$ nm and the laser pulse of 3 mJ energy is focused on the surface into a 1.8-μm spot (see [42] for details). Figure 3(a) compares the proton cutoff energy for various pulse durations measured in the experiment, simulations and provided by the analytical model Eqs. (1)–(3). All data sets agree well with each other. While the cutoff energy follows the measured and predicted flat scalings for long laser pulses, the details of the protons' spectral-angular distributions in Figs. 3(b)–3(d) reveal clear signatures of the TNSA process which severely degrades the resulting divergence. For $\tau_{\mathrm{las}} = 30$ fs, all protons remain well collimated, $\tau_{\mathrm{las}} = 100$ fs develops high divergence for slower protons, and $\tau_{\mathrm{las}} = 250$ fs generates a divergent TNSA beam. Note that this TNSA signature is much more pronounced in the modeling than in the experimental measurements, which we may explain by the specificity of the simulated 2D geometry. While the considered proton acceleration is essentially one-dimensional and should not depend significantly on the transverse dimensions, the 2D PIC simulations are known to greatly enhance the TNSA process and were shown to result in twice more efficient acceleration compared to the full 3D geometry [45].

We may refer to the described mechanism as radiation pressure assisted Coulomb explosion (RPACE). So far we have obtained the scaling of the maximum proton energies and have identified optimal conditions, but have also discovered that subsequent TNSA degrades the beam quality, thus limiting RPACE to the shorter laser durations. This process is governed by multiple parameters (laser intensity, duration, and ion composition), and one may expect that the rate of such degradation increases for higher laser energies as the electron temperature grows and TNSA intensifies. This tightens the limitation of RPACE with respect to the laser duration and imposes a suboptimal source performance with the maximum proton energy following the scaling Eq. (3). Practically, for a given laser energy and focusing geometry, the maximal pulse duration that preserves the low proton beam divergence should be found. In order to check the energy scaling, we consider a case with a laser of 30 mJ energy, 70 fs pulse duration, and 2.5 μm focal spot size. The simulated angular-spectral protons distribution is shown in Fig. 4 and indicates the energy cutoff at ≈2 MeV, which is in very good agreement with the expected cutoff at 1.9 MeV according to Eq. (3). While faster particles remain well collimated, Fig. 4 indicates that the protons with energies $W_p < 1.4$ MeV suffer the TNSA-induced increased divergence. We anticipate that in the full 3D geometry, this threshold should be well below 1 MeV. In Fig. 4, one may also note the angular

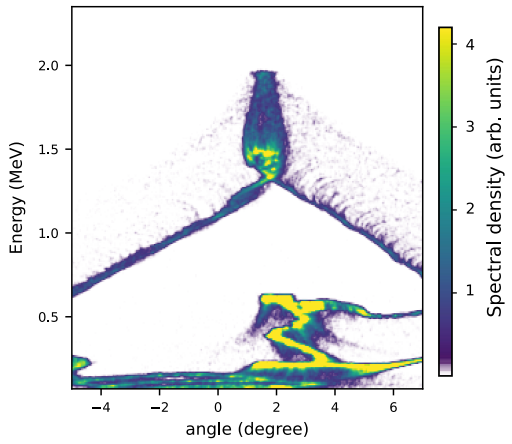

FIG. 4. Final angular-spectral distribution of protons for a laser energy of 30 mJ and 70 fs pulse duration.

modulations appearing for $W_p < 0.5$ MeV. These result from the surface plasma wave, which is excited by the laser and modulates the transverse spatial structure of the accelerating fields.

In summary, we have measured proton beams with unprecedented low divergence, generated at kHz repetition rate over a wide range of laser and plasma parameters. The divergence was found to be as low as 3° FWHM, about an order of magnitude smaller than thin foil TNSA proton beams. Proton energies reaching up to 0.48 ± 0.02 MeV for an optimal pulse duration ranging from 150 fs to 300 fs were measured with the steepest plasma-vacuum interface. The total charge reached a maximum of 98 ± 20 pC above 0.1 MeV, giving an average current of ~ 0.1 μA. The RPACE acceleration mechanism was identified in simulations and theory, showing that the surface protons Coulomb-explode after the laser radiation pressure evacuates preplasma electrons into the dense target. The scaling and optimal conditions for proton energies were obtained and discussed.

The demonstration of these unique proton beams is promising for numerous applications, some of which are within reach. Notable applications are ion implantation [46,47] and the production of radioisotopes for positron emission tomography (PET), which requires energies of a few MeV [48,49]. Such energies could be reached with readily available systems providing few-tens-mJ pulses according to our analysis.

This project has received funding from the European Union's Horizon 2020 research and innovation program under Grants Agreement No. 871124 (LaserLab-Europe) and No. 694596 (ERC Advanced Grant ExCoMet), as well as from the Agence Nationale de la Recherche (ANR) under Grant Agreement No. ANR-10-LABX-0039-PALM. This work was performed using HPC resources from CEA's Très Grand Centre de Calcul (TGCC) made available through the Grand Équipement Nationale de Calcul Intensif (GENCI) (Grant 2021-A0110510062). This research used the open-source particle-in-cell code, WarpX [50], primarily funded by the U.S. DOE Exascale Computing Project. We acknowledge all WarpX contributors.

[1] M. Roth, T. E. Cowan, M. H. Key, S. P. Hatchett, C. Brown, W. Fountain, J. Johnson, D. M. Pennington, R. A. Snavely, S. C. Wilks, K. Yasuike, H. Ruhl, F. Pegoraro, S. V. Bulanov, E. M. Campbell, M. D. Perry, and H. Powell, Phys. Rev. Lett. **86**, 436 (2001).

[2] P. K. Patel, A. J. Mackinnon, M. H. Key, T. E. Cowan, M. E. Foord, M. Allen, D. F. Price, H. Ruhl, P. T. Springer, and R. Stephens, Phys. Rev. Lett. **91**, 125004 (2003).

[3] M. Borghesi, D. H. Campbell, A. Schiavi, M. G. Haines, O. Willi, A. J. MacKinnon, P. Patel, L. A. Gizzi, M. Galimberti, R. J. Clarke, F. Pegoraro, H. Ruhl, and S. Bulanov, Phys. Plasmas **9**, 2214 (2002).

[4] V. Malka, J. Faure, Y. A. Gauduel, E. Lefebvre, A. Rousse, and K. T. Phuoc, Nat. Phys. **4**, 447 (2008).

[5] K. W. D. Ledingham, P. McKenna, and R. P. Singhal, Science **300**, 1107 (2003).

[6] E. Lefebvre, E. d'Humières, S. Fritzler, and V. Malka, J. Appl. Phys. **100**, 113308 (2006).

[7] U. Linz and J. Alonso, Phys. Rev. Accel. Beams **19**, 124802 (2016).

[8] S. C. Wilks, A. B. Langdon, T. E. Cowan, M. Roth, M. Singh, S. Hatchett, M. H. Key, D. Pennington, A. MacKinnon, and R. A. Snavely, Phys. Plasmas **8**, 542 (2001).

[9] T. Ceccotti, A. Lévy, H. Popescu, F. Réau, P. d'Oliveira, P. Monot, J. P. Geindre, E. Lefebvre, and P. Martin, Phys. Rev. Lett. **99**, 185002 (2007).

[10] M. Borghesi, in *Laser-Driven Sources of High Energy Particles and Radiation*, edited by L. A. Gizzi, R. Assmann, P. Koester, and A. Giulietti, Springer Proceedings in Physics 231 (Springer, Cham, 2019), pp. 143–164, 10.1007/978-3-030-25850-4_7.

[11] R. A. Snavely, M. H. Key, S. P. Hatchett, T. E. Cowan, M. Roth, T. W. Phillips, M. A. Stoyer, E. A. Henry, T. C. Sangster, M. S. Singh, S. C. Wilks, A. MacKinnon, A. Offenberger, D. M. Pennington, K. Yasuike, A. B. Langdon, B. F. Lasinski, J. Johnson, M. D. Perry, and E. M. Campbell, Phys. Rev. Lett. **85**, 2945 (2000).

[12] T. E. Cowan *et al.*, Phys. Rev. Lett. **92**, 204801 (2004).

[13] E. Brambrink, J. Schreiber, T. Schlegel, P. Audebert, J. Cobble, J. Fuchs, M. Hegelich, and M. Roth, Phys. Rev. Lett. **96**, 154801 (2006).

[14] T. Toncian, M. Borghesi, J. Fuchs, E. d'Humières, P. Antici, P. Audebert, E. Brambrink, C. A. Cecchetti, A. Pipahl, L. Romagnani, and O. Willi, Science **312**, 410 (2006).

[15] S. Kar, K. Markey, P. T. Simpson, C. Bellei, J. S. Green, S. R. Nagel, S. Kneip, D. C. Carroll, B. Dromey, L. Willingale, E. L. Clark, P. McKenna, Z. Najmudin, K. Krushelnick, P. Norreys, R. J. Clarke, D. Neely, M. Borghesi, and M. Zepf, Phys. Rev. Lett. **100**, 105004 (2008).

[16] S. Kar, H. Ahmed, R. Prasad, M. Cerchez, S. Brauckmann, B. Aurand, G. Cantono, P. Hadjisolomou, C. L. S. Lewis,

A. Macchi, G. Nersisyan, A. P. L. Robinson, A. M. Schroer, M. Swantusch, M. Zepf, O. Willi, and M. Borghesi, Nat. Commun. **7**, 10792 (2016).
[17] R. Sonobe, S. Kawata, S. Miyazaki, M. Nakamura, and T. Kikuchi, Phys. Plasmas **12**, 073104 (2005).
[18] S. Miyazaki, S. Kawata, R. Sonobe, and T. Kikuchi, Phys. Rev. E **71**, 056403 (2005).
[19] M. Nakamura, S. Kawata, R. Sonobe, Q. Kong, S. Miyazaki, N. Onuma, and T. Kikuchi, J. Appl. Phys. **101**, 113305 (2007).
[20] T. P. Yu, Y. Y. Ma, M. Chen, F. Q. Shao, M. Y. Yu, Y. Q. Gu, and Y. Yin, Phys. Plasmas **16**, 033112 (2009).
[21] K. H. Pae, I. W. Choi, S. J. Hahn, J. R. Cary, and J. Lee, Phys. Plasmas **16**, 073106 (2009).
[22] Y. Y. Ma, Z. M. Sheng, Y. Q. Gu, M. Y. Yu, Y. Yin, F. Q. Shao, T. P. Yu, and W. W. Chang, Phys. Plasmas **16**, 034502 (2009).
[23] M. Chen, A. Pukhov, T. P. Yu, and Z. M. Sheng, Phys. Rev. Lett. **103**, 024801 (2009).
[24] M. Chen, T.-P. Yu, A. Pukhov, and Z.-M. Sheng, New J. Phys. **12**, 045004 (2010).
[25] T. Okada, A. A. Andreev, Y. Mikado, and K. Okubo, Phys. Rev. E **74**, 026401 (2006).
[26] M.-P. Liu, H.-C. Wu, B.-S. Xie, J. Liu, H.-Y. Wang, and M. Y. Yu, Phys. Plasmas **15**, 063104 (2008).
[27] M. Ali Bake, B.-S. Xie, Shan-Zhang, and H.-Y. Wang, Phys. Plasmas **20**, 033112 (2013).
[28] N. Yasen, Y. Hou, L. Wang, H. Sang, M. A. Bake, and B. Xie, Plasma Sci. Technol. **21**, 045201 (2019).
[29] M. Matys, K. Nishihara, M. Kecova, J. Psikal, G. Korn, and S. V. Bulanov, High Energy Density Phys. **36**, 100844 (2020).
[30] O. Klimo, J. Psikal, J. Limpouch, and V. T. Tikhonchuk, Phys. Rev. ST Accel. Beams **11**, 031301 (2008).
[31] A. P. L. Robinson, M. Zepf, S. Kar, R. G. Evans, and C. Bellei, New J. Phys. **10**, 013021 (2008).
[32] B. Qiao, M. Zepf, M. Borghesi, and M. Geissler, Phys. Rev. Lett. **102**, 145002 (2009).
[33] H. B. Zhuo, Z. L. Chen, W. Yu, Z. M. Sheng, M. Y. Yu, Z. Jin, and R. Kodama, Phys. Rev. Lett. **105**, 065003 (2010).
[34] J. Park, S. S. Bulanov, J. Bin, Q. Ji, S. Steinke, J.-L. Vay, C. G. R. Geddes, C. B. Schroeder, W. P. Leemans, T. Schenkel, and E. Esarey, Phys. Plasmas **26**, 103108 (2019).
[35] K. H. Pae, H. Song, C.-M. Ryu, C. H. Nam, and C. M. Kim, Plasma Phys. Controlled Fusion **62**, 055009 (2020).
[36] B. Hou, J. Nees, J. Easter, J. Davis, G. Petrov, A. Thomas, and K. Krushelnick, Appl. Phys. Lett. **95**, 101503 (2009).
[37] M. Veltcheva, A. Borot, C. Thaury, A. Malvache, E. Lefebvre, A. Flacco, R. Lopez-Martens, and V. Malka, Phys. Rev. Lett. **108**, 075004 (2012).
[38] J. T. Morrison, S. Feister, K. D. Frische, D. R. Austin, G. K. Ngirmang, N. R. Murphy, C. Orban, E. A. Chowdhury, and W. M. Roquemore, New J. Phys. **20**, 022001 (2018).
[39] M. Ouillé, A. Vernier, F. Böhle, M. Bocoum, A. Jullien, M. Lozano, J.-P. Rousseau, Z. Cheng, D. Gustas, A. Blumenstein, P. Simon, S. Haessler, J. Faure, T. Nagy, and R. Lopez-Martens, Light **9**, 47 (2020).
[40] M. Bocoum, F. Böhle, A. Vernier, A. Jullien, J. Faure, and R. Lopez-Martens, Opt. Lett. **40**, 3009 (2015).
[41] A. Borot, D. Douillet, G. Iaquaniello, T. Lefrou, P. Audebert, J.-P. Geindre, and R. Lopez-Martens, Rev. Sci. Instrum. **85**, 013104 (2014).
[42] See Supplemental Material at http://link.aps.org/supplemental/10.1103/PhysRevAccelBeams.25.093402 for details on the experimental setup, supporting experimental results, and details on the PIC simulations and theoretical model.
[43] F. Brunel, Phys. Rev. Lett. **59**, 52 (1987).
[44] J.-L. Vay *et al.*, Phys. Plasmas **28**, 023105 (2021).
[45] E. d'Humières, A. Brantov, V. Yu. Bychenkov, and V. T. Tikhonchuk, Phys. Plasmas **20**, 023103 (2013).
[46] A. Lorusso, F. Belloni, D. Doria, V. Nassisi, J. Wolowski, J. Badziak, P. Parys, J. Krása, L. Láska, F. P. Boody, L. Torrisi, A. Mezzasalma, A. Picciotto, S. Gammino, L. Calcagnile, G. Quarta, and D. Bleiner, Nucl. Instrum. Methods Phys. Res., Sect. B **240**, 229 (2005).
[47] L. Torrisi, M. Cutroneo, A. Mackova, V. Lavrentiev, M. Pfeifer, and E. Krousky, Plasma Phys. Controlled Fusion **58**, 025011 (2016).
[48] S. Fritzler, V. Malka, G. Grillon, J. P. Rousseau, F. Burgy, E. Lefebvre, E. d'Humières, P. McKenna, and K. W. D. Ledingham, Appl. Phys. Lett. **83**, 3039 (2003).
[49] R. Clarke, S. Dorkings, D. Neely, and I. Musgrave, Laser acceleration of electrons, protons, and ions II; and medical applications of laser-generated beams of particles II; and harnessing relativistic plasma waves III, *Proceedings of the SPIE 8779, Prague, CZ* (SPIE, 2013), Vol. 8779, pp. 192–198, 10.1117/12.2016971.
[50] https://github.com/ECP-WarpX/WarpX.